J2J.4 A DUAL-DOPPLER ANALYSIS OF HURRICANE GUILLERMO (1997): INTERACTIONS BETWEEN THE EYE AND EYEWALL DURING RAPID INTENSIFICATION

Matthew D. Eastin*[1], Paul D. Reasor[2], Frank D. Marks Jr.[3], John F. Gamache[3]

[1] Department of Math and Computer Science, Central College, Pella, Iowa
[2] Department of Meteorology, The Florida State University, Tallahassee, Florida
[3] NOAA/AOML Hurricane Research Division, Miami, Florida

1. INTRODUCTION

The azimuthal distribution of hurricane inner-core deep convection often consists of multiple transient convective cells superimposed upon a quasi-persistent low-wavenumber structure. Numerous observations and numerical simulations suggest environmental vertical wind shear and internal dynamical processes significantly influence such azimuthal distribution (e.g., Reasor et al. 2000; Black et al. 2002; Corbosiero and Molinari 2002; Frank and Ritchie 1999, 2001; Kossin and Schubert 2001; Braun 2002). The vertical shear will induce a wavenumber-one asymmetry with enhanced convergence and ascent downshear. The more-transient higher-wavenumber "mesovortices", located along the eye-eyewall interface, will further enhance the ascent in those regions where mesovortical induced outflow converges with the low-level inflow associated with the environmental shear. Eastin et al. (2005a,b) recently demonstrated that a considerable fraction of the eyewall vertical mass transport was associated with transient, buoyant, convective-scale updrafts. In two hurricanes, the high equivalent potential temperatures (θ_e) observed in the buoyant updrafts at midlevels were only observed elsewhere in the low-level eye, suggesting an origin in the low-level eye and an association with mesovortical outflow. The objective of this study is to further elucidate the impact of evolving asymmetric vortical structures on the spatial distribution of hurricane inner-core convection through the aid of a unique dual-Doppler dataset and trajectory analysis.

2. DATA AND METHODS

Two NOAA P-3 aircraft observed the inner core of Hurricane Guillermo between 1800 and 2400 UTC on 2 August 1997. During this period, the hurricane was moving westward over $> 29°$C waters through moderate north-northwesterly vertical shear and was intensifying at an average rate of 2.4 mb hr^{-1} from an initial central pressure of 959 mb. Dual-Doppler velocity data was collected for ten passes through

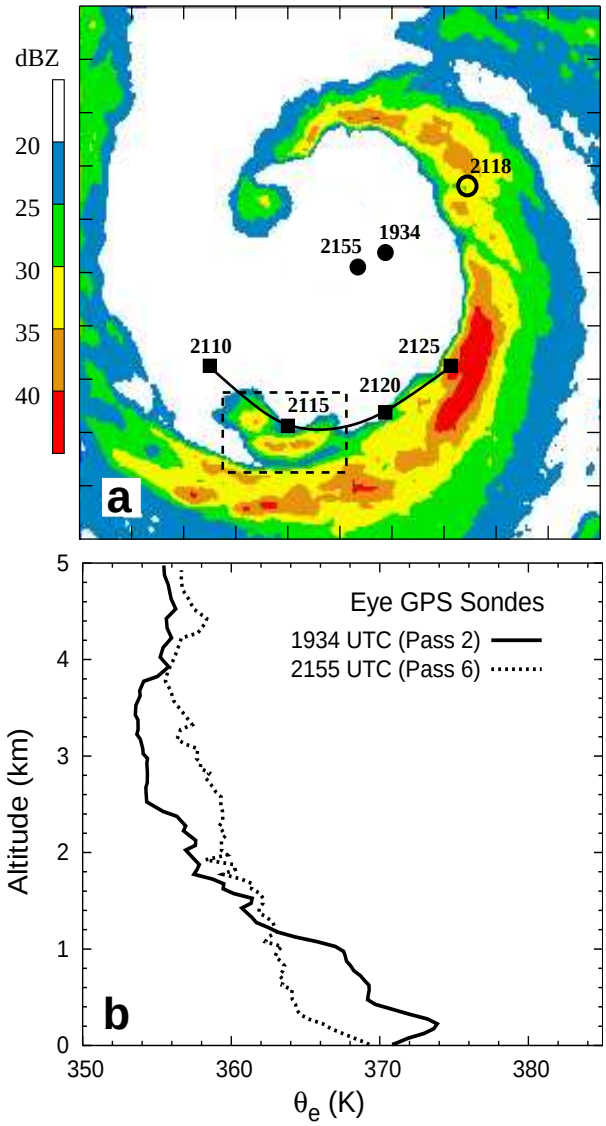

Figure 1: (a) Radar reflectivity at 5.5 km altitude at 2115 UTC during Pass 5 on 2 August. The domain is 100×100 km and tic marks are shown every 10 km. GPS dropsonde (filled circles), buoyant updraft core (open circle), and convective cell (filled squares) locations and times are also shown. (b) Profiles of θ_e obtained by the GPS sondes.

*Corresponding Author Address: Matthew D. Eastin, Department of Math and Computer Science, Central College, 812 University, Pella, IA 50219; email: eastinm@central.edu

the inner core at 3.0 and 5.5 km altitude. Currently, unique three-dimensional wind fields have been constructed for five of the ten passes following Gamache (1998). Each was decomposed into azimuthal mean and perturbation components following methods similar to Reasor et al. (2000). In contrast to previous Doppler radar studies of intense hurricanes, light precipitation within Guillermo's eye has permitted unprecedented wind field documentation throughout a large fraction of the eye.

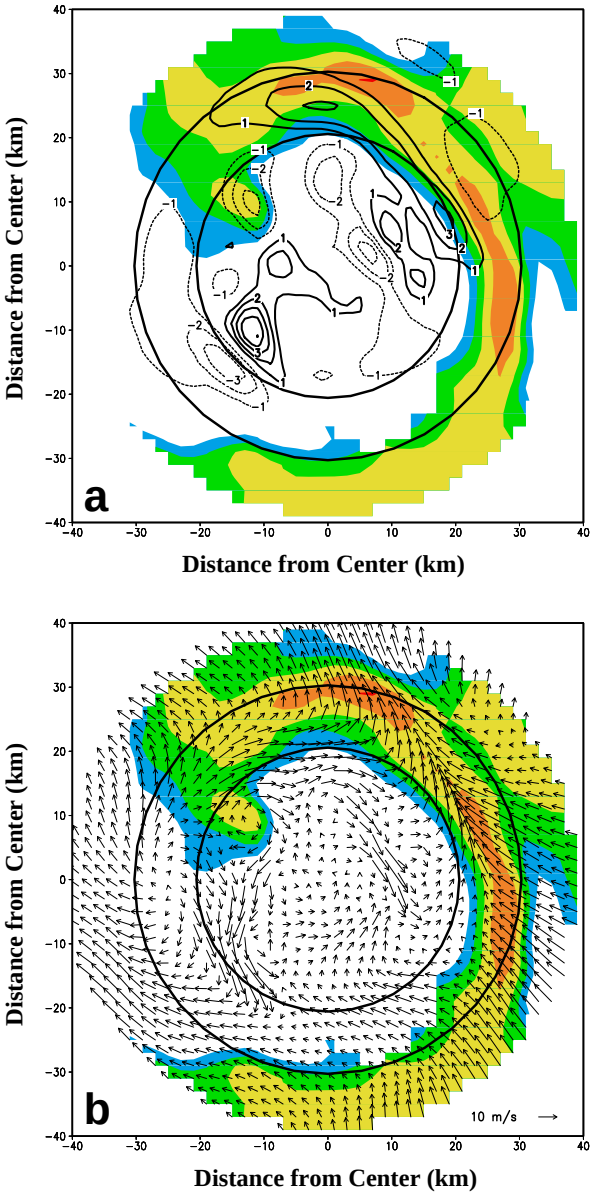

Figure 2: (a) Perturbation vorticity ($\times 10^{-3}$ s^{-1}) and (b) perturbation winds at 1 km altitude during Pass 5 on 2 August. Shaded contours show the 20, 25, 30, 35, and 40 dBZ levels of radar reflectivity. The 20 and 30 km range rings are also shown.

In order to document dynamic interactions between the eye and eyewall, several hundred three-dimensional air parcel trajectories were derived from each storm-relative dual-Doppler wind field following methods similar to Marks et al. (1992). Trajectories were calculated under the assumption that each wind field and the mean storm motion were in steady state. Initial "seed" locations were at each grid point (every 2 km) within 18 km of the circulation center at 0.5 km altitude (i.e., in the low-level eye; see Fig. 3). Trajectories were computed 5 h forward in time using a 30 s time step. The eye-eyewall boundary was broadly defined as a symmetric outward-sloping surface from 18 km radius at the ocean surface to 30 km radius at 12 km altitude (see Fig. 4), and was subjectively determined from radar reflectivity animations and cloud water contents at flight-level.

3. RESULTS AND DISCUSSION

The observations and results discussed here focus primarily on the fifth pass between 2106 and 2129 UTC. Radar animations from both aircraft depict a persistent wavenumber-one reflectivity pattern in the southern and eastern quadrants. At 2110 UTC a prominent convective cell developed along the inner

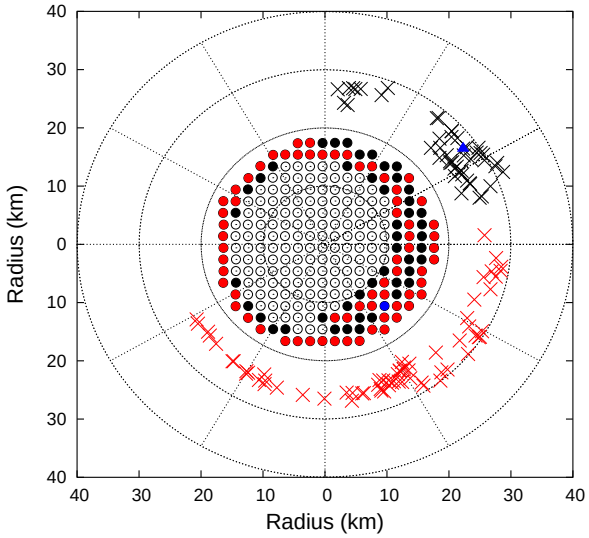

Figure 3: Trajectory seed locations at 0.5 km altitude within the eye (circles) and their subsequent locations at 5.5 km altitude within the eyewall (X's). Filled circles denote trajectories that escaped from the eye. Trajectories that did not escape (open circles) do not have a corresponding eyewall location. Red (black) symbols denote trajectories that were located in the southern (northeast) eyewall at 5.5 km altitude. Blue symbols denote the seed and eyewall locations for the trajectory shown in Fig. 4. Trajectories were calculated from the Pass 5 dual-Doppler wind field.

edge of the southwest eyewall (at ∼25 km radius; see Fig. 1a). By 2125 UTC the cell had tracked cyclonically around to the southeast and was merging with the wavenumber-one reflectivity pattern. After 2125 UTC the cell was untrackable as a unique feature.

The total perturbation vorticity (Fig. 2a) and wind (Fig. 2b) fields at 1 km altitude exhibit a rich asymmetric structure. Similar perturbation fields were also observed at 2, 3, and 4 km altitude. Of interest here, are the "mesovortices" in the southwest and northeast quadrants near the eye-eyewall interface, and their associated enhanced outflow from the eye. This outflow is converging with the southeasterly inflow associated with the environmental shear. In the case of the southwestern mesovortex, the outflow is roughly collocated with the convective cell development region (Fig 1a).

Roughly 45% of the 257 trajectories seeded in the low-level eye during Pass 5 "escaped" and ascended through the midlevel eyewall (Fig. 3). A typical escape trajectory is shown in Fig. 4. Several trajectories circumnavigated within the eye before escaping. Trajectories seeded as close as 10 km from the circulation center escaped. Most (88%) crossed the eye-eyewall boundary below 3 km in the northeast quadrant, and tracked cyclonically around the eyewall to the eastern quadrants while ascending to 5.5 km. Of the trajectories which escaped in the southwest quadrant (all below 3 km), most (94%) were located in the southwest eyewall upon ascending to 5.5 km (in the same region as the convective cell). The overall pattern of escape trajectory locations at 5.5 km altitude is striking similar to the radar reflectivity field at the same altitude (Fig. 1a), suggesting an intimate relationship between the azimuthal distribution of eyewall convection and mesovortical flow near the eye-eyewall interface.

Shown in Fig. 5 are the percent of trajectories seeded in the low-level eye which escaped and ascended through the midlevel eyewall as a function of seed radius for Passes 1, 2, 5, and 6. In general, escape percentages for Passes 1 and 2 were smaller than their respective counterparts during Passes 5 and 6, and the minimum seed radius for an escape trajectory was larger (∼12 km compared to ∼9 km, respectively). It should be noted that the perturbation vorticity structures (and mesovortical outflow) observed near the low-level eye-eyewall interface during Passes 1 and 2 (not shown) were relatively weaker. These results imply a direct relationship between the extent of mass export from the eye and the magnitude of the associated perturbation vorticity structures.

It is interesting to note that $\theta_e > 365$ K was predominant in the eye below 1 km during Pass 2 (at 1934 UTC in Fig. 1b) but not during Pass 6 (at 2155 UTC). Furthermore, as the aircraft passed through the northeast eyewall at 5.5 km altitude during Pass 5, a convective updraft exhibiting positive local buoyancy and $\theta_e > 368$ K was encountered at 2118 UTC (see Fig. 1a). The trajectory shown in Fig. 4 demonstrates that such a buoyant

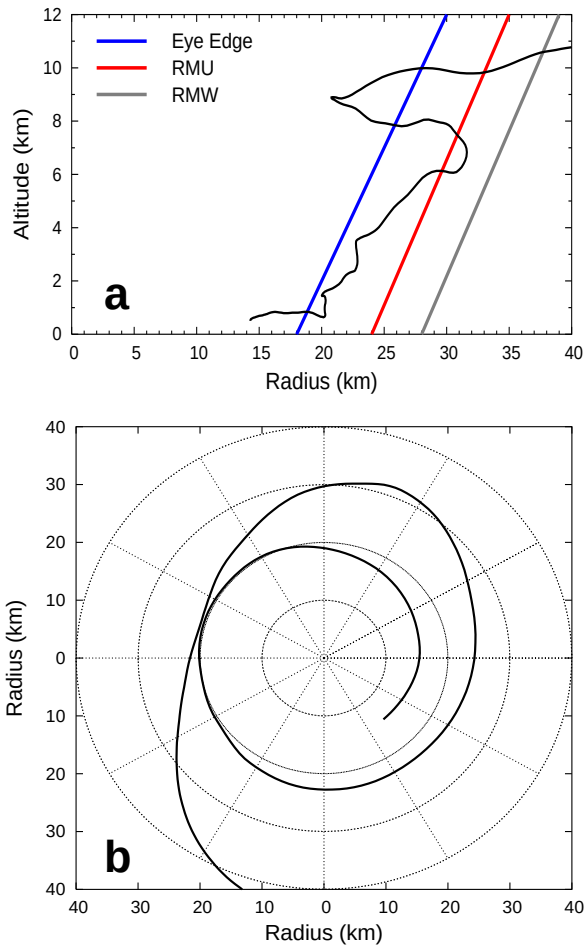

Figure 4: (a) Radius-altitude and (b) horizontal plan view perspectives for a typical "escape" trajectory. Also shown in (a) are the approximate eye-eyewall boundary, radius of maximum updraft (RMU), and radius of maximum tangential wind (RMW).

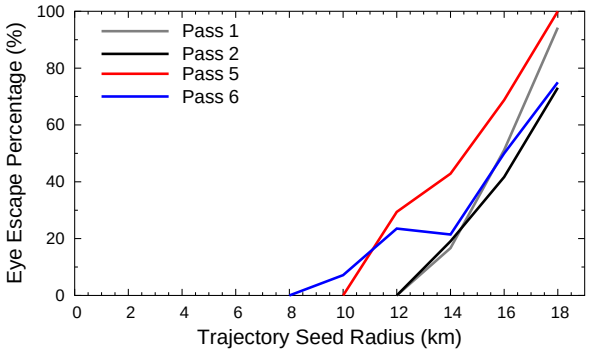

Figure 5: Percentage of trajectories seeded at 0.5 km altitude within the eye (inside r = 18 km) which escaped and were rising within the eyewall at 5.5 km altitude for Pass 1 (1845-1905 UTC), Pass 2 (1925-1944 UTC), Pass 5 (2106-2129 UTC), and Pass 6 (2144-2203 UTC).

updraft could have originated in the low-level eye. Of 14 eyewall updrafts encountered after Pass 5, several were positively buoyant but none exhibited $\theta_e >$ 366 K. While the convective updraft and convective cell cannot be uniquely associated with individual trajectories, these observations further imply a link between mesovortical flow across the eye/eyewall interface, the generation of buoyant eyewall convection, and the depletion of a high-θ_e reservoir in the low-level eye.

We have presented compelling observational evidence that significant mesovortical outflow from the low-level eye can help generate deep eyewall convection. Ongoing work involves the analysis of trajectories calculated from successive dual-Doppler wind fields linearly interpolated in time (i.e., a crude representation of an *evolving* wind field). Results presented by Kossin and Eastin (2001) and Prieto et al.(2001) from idealized numerical simulations suggest that the majority of air originating in the eye may be mixed outward into the eyewall within 24 h. Our current use of steady-state wind fields may underestimate the actual numbers of escape trajectories. Future work will also address trajectories seeded within and outside the eyewall.

Acknowledgments: Funding for this research was partially provided by the National Science Foundation and the National Research Council.

REFERENCES

Black, M. L., J. F. Gamache, F. D. Marks, Jr., C. E. Samsury, and H. E. Willoughby, 2002: Eastern Pacific Hurricanes Jimena of 1991 and Olivia of 1994: The effect of vertical shear on structure and intensity. *Mon. Wea. Rev.*, **130**, 2291-2312.

Braun, S. A., 2002: A cloud-resolving simulation of Hurricane Bob (1991): Storm structure and eyewall buoyancy. *Mon. Wea. Rev.*, **130**, 1573-1592.

Corbosiero, K. L., and J. Molinari, 2002: The effects of vertical wind shear on the distribution of convection in tropical cyclones. *Mon. Wea. Rev.*, **130**, 2110-2123.

Eastin, M. D., W. M. Gray, and P. G. Black, 2005a: Buoyancy of convective vertical motions in the inner core of intense hurricanes. Part I: General Statistics. *Mon. Wea. Rev.*, **133**, 188-208.

Eastin, M. D., W. M. Gray, and P. G. Black, 2005b: Buoyancy of convective vertical motions in the inner core of intense hurricanes. Part II: Case Studies. *Mon. Wea. Rev.*, **133**, 209-227.

Frank, W. M., and E. A. Ritchie, 1999: Effects of environmental flow upon tropical cyclone structure. *Mon. Wea. Rev.*, **127**, 2044-2061.

Frank, W. M., and E. A. Ritchie, 2001: Effects of vertical wind shear on the intensity and structure of numerically simulated hurricanes. *Mon. Wea. Rev.*, **129**, 2249-2269.

Kossin, J. P., and M. D. Eastin, 2001: Two distinct regimes in the kinematic and thermodynamic structure of the hurricane eye and eyewall. *J. Atmos. Sci.*, **58**, 1079-1090.

Kossin, J. P., and W. H. Schubert, 2001: Mesovortices, polygonal flow patterns, and rapid pressure falls in hurricane-like vortices. *J. Atmos. Sci.*, **58**, 2196-2209.

Gamache, J. F., 1998: Evaluation of a fully three-dimensional variational Doppler analysis technique. Preprints, *28th Conf. on Radar Meteorology*, Austin, TX, Amer. Meteor. Soc., 422-423.

Marks, F. D., Jr., R. A. Houze, Jr., and J. F. Gamache, 1992: Dual-aircraft investigation of the inner core of Hurricane Norbert. Part I: Kinematic structure. *J. Atmos. Sci.*, **49**, 919-942.

Prieto, R., J. P. Kossin, and W. H. Schubert, 2001: Symmetrization of lopsided vorticity monopoles and offset hurricane eyes. *Quart. J. Roy. Meteor. Soc.*, **127**, 1-20.

Reasor, P. D., M. T. Montgomery, F. D. Marks Jr., and J. F. Gamache, 2000: Low-wavenumber structure and evolution of the hurricane inner core observed by airborne dual-Doppler radar. *Mon. Wea. Rev.*, **128**, 1653-1680.